ORNL/TM-6637
ENDF-280

Status of ENDF/B-V Neutron Emission Spectra Induced by 14-MeV Neutrons

D. M. Hetrick
D. C. Larson
C. Y. Fu

OAK RIDGE NATIONAL LABORATORY
OPERATED BY UNION CARBIDE CORPORATION · FOR THE DEPARTMENT OF ENERGY

Printed in the United States of America. Available from
National Technical Information Service
U.S. Department of Commerce
5285 Port Royal Road, Springfield, Virginia 22161
Price: Printed Copy $4.50; Microfiche $3.00

ORNL/TM-6637
ENDF-280

Contract No. W-7405-eng-26

Engineering Physics Division

STATUS OF ENDF/B-V NEUTRON EMISSION SPECTRA INDUCED BY 14-MeV NEUTRONS

D. M. Hetrick,* D. C. Larson, and C. Y. Fu

*Computer Science Division

Date Published - April 1979

Prepared by the
OAK RIDGE NATIONAL LABORATORY
Oak Ridge, Tennessee 37830
operated by
UNION CARBIDE CORPORATION
for the
DEPARTMENT OF ENERGY

CONTENTS

ABSTRACT

ENDF/B-V neutron emission spectra induced by 14.6 MeV incident neutrons are graphically compared with experimental data. The elements selected for the comparisons include Na, Mg, Al, Si, Ca, Ti, V, Cr, Fe, Ni, Cu, Nb, W, and Pb. Partial as well as total spectra from the ENDF/B-V evaluations are shown in each graph, while experimental data were available only for the total. Energy distribution laws utilized for the reaction types in each element are explained. Agreement between evaluated and experimental data is discussed, and recommendations for improvements are made. In general, evaluations which utilized advanced nuclear model codes, including precompound effects, agree well with measured spectra.

I. INTRODUCTION

Graphical comparisons of ENDF/B-V neutron emission spectra with experimental data induced by 14-MeV incident neutrons are presented. The elements chosen for the comparisons are those considered important for fusion reactor applications. On each graph, partial and total emission spectra from the ENDF/B-V files are shown. Thus, disagreement with the experimental data, if any, may be attributed to specific partial cross sections. Experimental data are available only for the total emission spectra.

The elements chosen for the present study include Na, Mg, Al, Si, Ca, Ti, V, Cr, Fe, Ni, Cu, Nb, W, and Pb. Energy distribution laws used for constructing the neutron probability distribution in each element are explained in detail.

Experimental data used in this work are those by Hermsdorf et al.[1] We have found from several of our evaluations that these data are generally consistent with isolated results of others. For simplicity and general consistency, we show this set of data for all comparisons. For a few others, the data of Clayeux and Voignier[2] are also shown.

Deficiencies in the ENDF/B-V neutron emission spectra for several materials are uncovered and discussed.

II. EXPERIMENTAL DATA

Experimental data given by Hermsdorf et al.[1] and Clayeux and Voignier[2] were utilized for this work. There are numerous other data sets available, but since they are generally in agreement with data of Hermsdorf et al.,

they have been left off the plots for the purpose of clarity. However, the data of Clayeux and Voignier have been included since they have been used frequently for evaluation work, and since they sometimes differ significantly from the data of Hermsdorf et al. and others, we felt it useful to include them for comparison. In addition, the integrated cross sections obtained from data of Clayeux and Voignier are much larger than the calculated results, due to the large number of low energy neutrons present in their work.

In their report, Hermsdorf et al. presented the center-of-mass angular distributions of secondary neutrons integrated over 1.0-MeV energy intervals. We have fitted a series of Legendre coefficients by least squares to the angular data for elements Na, Mg, Al, Si, Ca, Ti, V, Cr, Fe, Ni, Cu, Nb, W, and Pb for each energy interval given. For each energy interval, the integrated cross section was computed for different polynomial orders to obtain the total differential cross section. The integral obtained from the order that gave the best visual fit (generally $\ell = 3$) was compared with evaluated data. The calculated differential cross sections resulting from this procedure are given in Tables 1 - 3 in the Appendix for the above elements. Graphical results are presented in Figs. 1 - 17. The error bars shown in these tables and figures correspond to the errors given in the report by Hermsdorf et al. plus their estimated 10% systematic error.

The data of Clayeux and Voignier were taken directly from tables in their report. Whereas Hermsdorf et al. obtained cross sections from the bombardment of the materials by 14.6-MeV neutrons, Clayeux and Voignier's data were given for 14.0-MeV neutrons. Data of Clayeux and Voignier for the elements Mg, Al, Si, Ca, Fe, Ni, Cu, and Pb were used in this paper.

III. ENDF/B-V FILES

In Figs. 1 - 17 the differential cross sections versus outgoing neutron energy are plotted for all reaction types that produce secondary neutrons. In all figures, the incident neutron energy was 14.6 MeV. The differential cross section for each reaction type was obtained from

$$\frac{d\ (E\rightarrow E')}{dE'} = m\ \sigma(E)\ p(E\rightarrow E') \qquad (1)$$

as given in Ref. 3.

Here $\sigma(E)$ is the cross section for incident energy E as given in File 3 of the ENDF/B-V library, m is the neutron multiplicity, and $p(E\rightarrow E')$ represents the energy distribution for the secondary particle. The energy distribution is broken down into partial energy distributions,[3]

$$p(E\rightarrow E') = \sum_{k=1}^{NK} p_k(E)\ f_k(E\rightarrow E')\ , \qquad (2)$$

where $f_k(E\rightarrow E')$ represents the distributions of the secondary neutron energies E' calculated from data given in File 5 of the library. At a particular incident neutron energy E,

$$\sum_{k=1}^{NK} p_k(E) = 1, \qquad (3)$$

where $p_k(E)$ is the fractional probability that the distribution $f_k(E\rightarrow E')$ applies at E. NK is the number of partial distributions, and, with the exception of reaction types for the elements Ni, W-182, W-183, W-184, and W-186, is equal to 1.

The energy distributions $f_k(E \rightarrow E')$ are described by different analytical formulations. Each formulation, or energy distribution law, has an identification number (LF number) associated with it.[3] A summary of what distribution law was used in the evaluation for each reaction type, for each material, is given in Section IV. Figures 1-17 display the total differential cross section obtained by summing the curves from all neutron producing reactions present in the evaluation. This total neutron emission cross section is compared with the data of Hermsdorf et al.[1] and Clayeux and Voignier.[2]

IV. DISTRIBUTION LAWS FOR EACH ELEMENT

Sodium

The results for the element sodium are shown in Fig. 1. For the (n,n′) continuum cross section curve (MT = 91 in ENDF/B-V library), the energy distribution $f(E \rightarrow E')$ was calculated by using the evaporation spectrum (LF = 9; see ref. 3). That is, the distribution was obtained by the formula

$$f(E \rightarrow E') = \frac{E'}{I} e^{-\frac{E'}{\theta}} \tag{4}$$

where I is the normalization constant

$$I = \theta^2 \left[1 - e^{-\left(\frac{E - U}{\theta}\right)} \left(1 + \frac{E - U}{\theta}\right) \right]. \tag{5}$$

θ, the effective nuclear temperature, was retrieved from File 5 where it was tabulated as a function of incident neutron energy E. The constant U, also obtained from File 5, defined the proper limit for the outgoing neutron energy by

$$0 \leq E' \leq E - U \ . \tag{6}$$

The neutron energies E′ in Eq. (4) were taken as the midpoints of 0.1 MeV bins with the maximum defined by (6). The cross section $\sigma(E)$ [see Eq. (1)] was calculated for an incident energy of 14.6 MeV by interpolation. This cross section, along with the energy distribution, was substituted into Eq. (1) to obtain the desired result. The same method was used in the computations for the (n,2n) (MT=16) reaction. Cross sections for all discrete levels except the first excited state (MT = 51 in File 3) at 0.440 MeV were zero in the evaluation for incident neutron energies greater than 12 MeV. For this excited state, the cross section was calculated for an incident energy of 14.6 MeV by interpolation and the outgoing neutron energy was calculated by subtracting the reaction Q-value from the incident energy. The resulting curve is labeled (n,n′) discrete. Note that this curve results from using a 1.0-MeV bin for the calculation. The above reaction types were summed via linear-linear interpolation and the resulting curve is labeled (TOTAL) in the figure. Thus the total neutron emission cross section at 14.6 MeV consists of the (n,2n) plus (n,n′) continuum, plus the cross section for the 0.440-MeV level.

Magnesium

The results for magnesium are shown in Fig. 2. The evaporation spectrum (LF = 9) was used to compute the energy distribution for neutrons from the (n,nα) (MT = 22) and (n,np) (MT = 28) cross sections. For the (n,2n) cross section curve, a set of incident energy points E_i was given, and $f(E_i \rightarrow E')$ was tabulated as a function of E' in File 5 of the ENDF/B-V library; i.e., LF was equal to 1 (see ref. 3). The energy distribution $f(E_i \rightarrow E')$ and cross section $\sigma(E_i)$ were calculated for an incident energy equal to 14.6 MeV by interpolation and were substituted into Eq. (1) to obtain the desired result. The same procedure was used for the (n,n′) continuum cross section curve. Data for the inelastic level excitation cross sections were given for 40 levels (MT = 51 thru 90) in File 3, with a maximum outgoing neutron energy of 14.016 MeV. For each excited state, the cross section was calculated for an incident energy of 14.6 MeV by interpolation and the outgoing neutron energy was calculated by subtracting the reaction Q-value from the incident energy. These results were combined into 1.0-MeV bins. It is noted here that the observed structure of the (n,n′) discrete curve may be misleading since the peak height for each bin depends on the bin width.

Aluminum

The energy distribution $f(E \rightarrow E')$ for the (n,2n) cross section for aluminum (see Fig. 3) was computed by using the LF = 1 formulation. File 3 of the ENDF/B-V library included data for 31 excited states (MT = 51 thru 81), and the maximum outgoing neutron energy for these discrete levels was given as 13.757 MeV. The same methods as discussed above were used to compute the cross section curves for this element.

Silicon

The results for the element silicon are shown in Fig. 4. The energy distribution law with identification LF = 1 was used to compute the distributions for outgoing neutrons from the (n,nα), (n,np), and (n,n′) continuum reactions, while the evaporation spectrum (LF = 9) was used to determine the distribution for the (n,2n) curve. Data for the inelastic level excitation cross sections were given for 22 levels (MT = 51 thru 72) in File 3, with a maximum outgoing neutron energy of 13.327 MeV. The same procedure as described above was used to calculate the (n,n′) discrete cross section curve.

Calcium

The simple fission or Maxwellian spectrum was specified to compute the energy distribution $f(E \to E')$ for the (n,2n) cross section curve for calcium (LF = 7; see ref. 3). These results are shown in Fig. 5. The distribution was determined by the formula

$$f(E \to E') = \frac{\sqrt{E'}}{I} e^{-\frac{E'}{\theta}} . \tag{7}$$

Here, I is the normalization constant

$$I = \theta^{\frac{3}{2}} \left[\frac{\sqrt{\pi}}{2} \operatorname{erf} \left(\sqrt{\frac{E - U}{\theta}} \right) - \sqrt{\frac{E - U}{\theta}} \, e^{-\left(\frac{E - U}{\theta}\right)} \right] . \tag{8}$$

As for the evaporation energy distribution law LF = 9, θ is the effective nuclear temperature and U is a constant that defines the proper limit for the outgoing neutron energy [see Eq. (6)]. The neutron energies E′ [Eq. (7)] were taken as the midpoints of 0.2 MeV bins with the limits defined

by Eq. (6). For neutrons from the (n,nα) cross section, the (n,np) cross section, and the (n,n′) continuum, the energy distributions were interpolated from the tabulated distribution (LF = 1). File 3 of the ENDF/B-V library included data for 23 excited states (MT = 51 thru 73) with the maximum outgoing neutron energy being 13.442 MeV. The (n,n′) discrete curve was determined by the same procedure as discussed previously.

Titanium

Figure 6 shows the results obtained for titanium. The LF = 1 formulation was used to calculate energy distributions for the (n,2n) and (n,n′) continuum cross section curves while the evaporation spectrum law (LF = 9) was used in computing the neutron distributions for the (n,nα) and (n,np) reactions. Data for the inelastic level excitation cross sections were given for 3 levels (MT = 51 thru 53) with a maximum outgoing neutron energy of 14.441 MeV. The same algorithms as discussed above were used to compute the cross section curves for this element.

Vanadium

The Maxwellian spectrum (LF = 7) was used to calculate the energy distribution f(E→E′) for neutrons from the (n,2n) reaction for vanadium (see Fig. 7). For both the (n,nα) and (n,np) cross sections, the energy distributions were computed by the evaporation spectrum law (LF = 9), while the (n,n′) continuum curve was interpolated from the tabulated distribution (LF = 1). File 3 of the ENDF/B-V library contains data for 7 excited states (MT = 51 thru 57) with the maximum outgoing neutron energy being 14.28 MeV. Again, see the discussion under the element magnesium above for the procedures in calculating the (n,n′) discrete curve.

Chromium

Figure 8 shows results obtained for chromium. The LF = 1 formulation was used to compute the energy distribution for the (n,n′) continuum, while the evaporation spectrum (LF = 9) was used to calculate the energy distributions for neutrons from the (n,2n), (n,nα), and (n,np) reactions. For the discrete levels, File 3 of the ENDF/B-V library included data for 40 excited states (MT = 51 thru 90) with the maximum outgoing neutron energy being 14.036 MeV. All computations for this element were consistent with the calculations described in the above discussions.

Iron

The results for iron are given in Fig. 9. The LF = 1 formulation was used to calculate the energy distributions for the (n,2n), (n,nα), (n,np), and (n,n′) continuum reactions. File 3 of the ENDF/B-V library includes data for 26 excited states (MT = 51 thru 76), and the maximum outgoing neutron energy for these discrete levels was given as 13.754 MeV. The same methods as discussed above were used to compute the cross section curves for this element.

Nickel

The evaporation spectrum (LF = 9) was used to compute the energy distributions for neutrons from the (n,2n), (n,nα), and (n,np) reactions for nickel (see Fig. 10). It is noted here that NK in Eq. (2) and (3) was equal to 2 in the ENDF/B-V library for the (n,2n) reaction since two different nuclear temperatures were used for each incident energy. For the (n,n′) continuum cross section curve, the distribution law with identity LF = 1 was used to calculate the energy distribution. The

inelastic level excitation cross sections were given for 26 levels (MT = 51 thru 76) with a maximum outgoing neutron energy of 14.53 MeV. The same procedure as discussed for the element magnesium above was used to determine the (n,n′) discrete curve shown in the figure.

Copper

Figure 11 shows the results obtained for copper. The energy distributions $f(E \rightarrow E')$ for the (n,n′) continuum and (n,2n) cross section curves were calculated by using the energy distribution law with the identification LF = 1 (see above). For neutrons from the (n,np) and (n,nα) reactions, the evaporation spectrum law (LF = 9) was used to obtain the energy distributions. The inelastic level excitation cross sections were given for 11 levels (MT = 51 thru 61) with a maximum outgoing neutron energy of 13.93 MeV. Again, the same steps were used for the calculation of the (n,n′) discrete curve as discussed for the element magnesium above.

Niobium

The results for the element niobium are given in Fig. 12. The LF = 1 formulation was used to calculate energy distributions for neutrons from the (n,2n), (n,nα), and (n,n′) continuum reactions. For each discrete level, the cross section (File 3) was zero for an incident neutron energy of 14.6 MeV. Thus, the (n,n′) curve for niobium is totally from the continuum. The same methods as discussed above were used to compute the cross section curves for this material.

Tungsten

The energy distributions for neutrons from the (n,2n), (n,3n) (MT = 17 in ENDF/B-V library), (n,np), and (n,n′) continuum reactions for tungsten, shown for 4 isotopes in Figs. 13 - 16, were calculated by using the evaporation spectrum (LF = 9). For an incident neutron energy of 14.6 MeV, the inelastic level excitation cross section was given for only 1 level (MT = 51) for W-182, W-184, and W-186; the cross sections were given for 2 levels (MT = 51 and 52) for W-183. The other discrete levels had cross sections of zero for an incident energy of 14.6 MeV. The maximum outgoing neutron energy ranged from 14.48 MeV for W-186 to 14.55 MeV for W-183. All computations for tungsten were consistent with the calculations described in the elements above. However, NK [in Eqs. (2) and (3)] was equal to 2 for the (n,2n) and (n,np) reactions and equal to 3 for the (n,3n) reaction in the data for each isotope since various nuclear temperatures were used for each incident neutron energy.

Lead

Figure 17 shows the results obtained for lead. The LF = 1 formulation was used to compute the energy distributions for the (n,2n), (n,3n), and the (n,n′) continuum reactions. For the discrete levels, File 3 included data for 35 excited states (MT = 51 thru 85) with a maximum outgoing neutron energy of 14.03 MeV. All calculations for lead were consistent with the computations described in the above elements.

V. DISCUSSIONS AND CONCLUSION

Sodium (Fig. 1)

The evaluation is in reasonable agreement with the data of Hermsdorf. However, outgoing neutrons with energies greater than 6.5 MeV are underestimated by about 30%, indicating the lack of a precompound component. Only one discrete level, at 0.44 MeV, has a nonzero cross section at E_n = 14.6 MeV.

Magnesium (Fig. 2)

The data sets of Clayeux and Hermsdorf are in disagreement, with the evaluation lying approximately between them. The evaluation somewhat underestimates (see ref. 4) a 14 MeV pulsed sphere measurement performed at Livermore, indicating that the Hermsdorf data is probably correct. The evaluation also underestimated this data set at most neutron energies by 30% to 40%, and would benefit by the inclusion of a precompound component.

Aluminum (Fig. 3)

For this material, data of Clayeux and Hermsdorf are in good agreement. However, there are too few neutrons below 2 MeV in the evaluation. This may be caused by omission of neutrons from the (n,pn) and (n,αn) reactions. The evaluation also overestimates the number of neutrons with energies greater than 6 MeV.

Silicon (Fig. 4)

The evaluation for silicon needs more neutrons from 6 to 8 MeV, but otherwise is in good agreement with both data sets.

Calcium (Fig. 5)

The two data sets shown are in sharp disagreement for Ca. From the fact that a precompound component has not been included in the evaluation (see ref. 5), it may be concluded that the evaluated spectrum is somewhat short of high energy neutrons and the Clayeux data for Ca are in serious error.

Iron (Fig. 9)

The evaluated spectrum is in good agreement with the experimental data. The evaluation of various partial neutron production spectra was based on an advanced nuclear model analysis[6] of several measured total neutron production spectra.

Copper (Fig. 11)

The evaluated spectrum needs more high energy neutrons between 8 and 13 MeV.

Lead (Fig. 17)

There is good agreement between the evaluation and the data. The evaluation had adequate data support, and was coupled with a nuclear model analysis.[7] The bump in the (n,n′) spectrum near 1 MeV reflects the use of a giant dipole for the gamma-ray channels in the calculation.

Titanium, Vanadium, Chromium, Nickel, Niobium, Tungsten

These materials appear to have similar deficiencies in their neutron spectra. First, there are too many neutrons in the (n,n′) spectrum above the (n,2n) threshold. This indicates that competition between the neutron channels in the (n,2n) reaction and the gamma-ray channels in the (n,n′γ) reaction does not seem to have been considered properly. Second, there are too few (or too many in the case of Nb) high energy neutrons, indicating that precompound and/or direct interaction effects have not been treated correctly in model calculations or were based on inadequate estimates. It appears that both deficiencies can be removed by using one of the recently developed nuclear model codes, GNASH[8] or TNG.[9] An early version of TNG was used for the analysis of neutron spectra for Fe and Pb, showing reasonable success as evidenced in this report.

From the discussions above we conclude that the ENDF/B-V evaluations for the neutron spectra resulting from 14.6-MeV neutron interactions are reasonably good for Fe and Pb and fair for Na, Al, and Si. Further evaluation is required for Mg, Ca, Ti, V, Cr, Ni, Cu, Nb, W-182, W-183, W-184, and W-186. From the nature of the deficiencies shown we recommend that advanced nuclear model codes[8,9] employing precompound emission be used in future evaluations to assure consistency amoung various partial cross sections and spectra and for extrapolating to energy ranges in which measurements have not been made.

REFERENCES

1. D. Hermsdorf, A. Meister, S. Sassonoff, D. Seeliger, K. Seidel, and F. Shahin, Zentralinstitut Für Kernforschung Rossendorf Bei Dresden, ZfK-277 (Ü), (1975).
2. G. Clayeux and J. Voignier, Centre d 'Etudes de Limeil CEA-R-4279 (1972).
3. D. Garber, C. Dunford, and S. Pearlstein, "Data Formats and Procedures for the Evaluated Nuclear Data File, ENDF," ENDF-102, BNL-NCS-50496, (1975).
4. M. K. Drake and M. P. Fricke, Defense Nuclear Agency Report DNA 3479F (1975).
5. C. Y. Fu, Atomic Data and Nuclear Data Tables 17, 127 (1976).
6. C. Y. Fu, "Development of a Two-Step Hauser-Feshbach Code with Precompound Decays and Gamma-Ray Cascades: A Theoretical Tool for Cross Section Evaluations," Conf. Proc. Nuclear Cross Sections and Technology, Washington, D. C. 1975, NBS-SP-425, p. 328 (1975).
7. C. Y. Fu, private communication (1978).
8. E. D. Arthur and P. G. Young, "Cross Sections in the Energy Range from 10 to 40 MeV calculated with the GNASH Code," Symp. on Neutron Cross Sections from 10 to 40 MeV, Brookhaven National Laboratory, Upton, New York, 1977, eds. M. R. Bhat and S. Pearlstein, BNL-NCS-50681, p. 467 (1977).
9. C. Y. Fu, "Multi-Step Hauser-Feshbach Codes with Precompound Effects: A Brief Review of Current and Required Developments and Applications up to 40 MeV," ibid, p. 453 (1977).

APPENDIX

This Appendix provides tables giving the integrated cross sections of all energy levels as obtained from Legendre fits to the data of Hermsdorf et al.[1] for the elements Na, Mg, Al, Si, Ca, Ti, V, Cr, Fe, Ni, Cu, Nb, W, and Pb.

TABLE 1. Integrated Cross Sections for the Elements Na, Mg, Al, and Si.

Energy Interval (MeV)	Integrated Cross Section (Mb/MeV)			
	Na	Mg	Al	Si
2.0 - 3.0	118.3 ± 14.9	143.7 ± 17.6	150.4 ± 18.5	92.2 ± 12.5
3.0 - 4.0	92.0 ± 11.6	86.3 ± 11.0	112.9 ± 14.0	82.2 ± 9.8
4.0 - 5.0	79.3 ± 10.0	57.3 ± 7.6	87.0 ± 10.6	65.3 ± 8.0
5.0 - 6.0	68.5 ± 8.7	60.3 ± 7.7	66.6 ± 8.3	53.1 ± 6.6
6.0 - 7.0	65.2 ± 7.8	51.9 ± 6.6	50.5 ± 6.4	46.2 ± 5.4
7.0 - 8.0	53.3 ± 6.2	36.7 ± 4.7	40.2 ± 5.2	40.7 ± 4.9
8.0 - 9.0	36.6 ± 4.5	32.2 ± 4.2	30.6 ± 4.0	20.0 ± 2.5
9.0 - 10.0	27.4 ± 3.7	29.1 ± 3.7	25.1 ± 3.2	18.1 ± 2.3
10.0 - 11.0	22.9 ± 3.0	23.7 ± 3.2	18.0 ± 2.4	17.4 ± 2.4

TABLE 2. Integrated Cross Sections for the Elements Ca, Ti, V, Cr, and Fe.

Energy Interval (MeV)	Integrated Cross Section (Mb/MeV)				
	Ca	Ti	V	Cr	Fe
2.0 - 3.0	154.7 ± 17.8	320.4 ± 34.8	246.4 ± 26.0	217.3 ± 25.2	196.8 ± 24.1
3.0 - 4.0	91.5 ± 10.8	187.5 ± 20.9	155.7 ± 16.5	161.2 ± 19.3	123.7 ± 15.2
4.0 - 5.0	67.4 ± 7.9	100.9 ± 11.4	78.7 ± 8.6	118.0 ± 14.6	84.8 ± 10.6
5.0 - 6.0	55.6 ± 6.5	67.2 ± 7.8	59.6 ± 6.6	90.8 ± 11.3	56.7 ± 7.0
6.0 - 7.0	45.3 ± 5.4	54.9 ± 6.6	47.6 ± 5.3	70.3 ± 8.7	39.9 ± 5.0
7.0 - 8.0	51.9 ± 6.0	47.9 ± 5.5	39.1 ± 4.4	59.6 ± 7.2	30.3 ± 3.9
8.0 - 9.0	38.7 ± 4.6	36.5 ± 4.5	29.3 ± 3.3	38.6 ± 4.9	23.4 ± 3.0
9.0 - 10.0	39.2 ± 4.7	28.0 ± 3.4	21.3 ± 2.4	27.2 ± 3.6	18.6 ± 2.5
10.0 - 11.0	51.3 ± 5.9	17.4 ± 2.0	11.4 ± 1.3	19.5 ± 2.6	11.9 ± 1.6

TABLE 3. Integrated Cross Sections for the Elements Ni, Cu, Nb, W, and Pb.

Energy terval (MeV)	Integrated Cross Section (Mb/MeV)				
	Ni	Cu	Nb	W	Pb
2.0 - 3.0	149.1 ± 18.3	243.1 ± 30.0	610.0 ± 65.0	416.9 ± 45.4	705.8 ± 73.3
3.0 - 4.0	95.1 ± 11.7	164.1 ± 20.2	303.6 ± 33.0	178.8 ± 20.9	368.6 ± 39.3
4.0 - 5.0	63.8 ± 8.0	95.0 ± 11.9	131.9 ± 14.6	92.1 ± 11.5	180.3 ± 20.0
5.0 - 6.0	45.0 ± 5.6	62.1 ± 7.8	84.9 ± 9.6	64.1 ± 8.1	98.8 ± 11.4
6.0 - 7.0	32.7 ± 4.2	45.5 ± 5.7	53.8 ± 6.2	54.5 ± 6.8	71.3 ± 8.4
7.0 - 8.0	26.1 ± 3.3	28.6 ± 3.6	44.4 ± 5.2	53.6 ± 6.5	61.2 ± 7.2
8.0 - 9.0	19.6 ± 2.6	22.9 ± 2.9	24.2 ± 3.0	56.2 ± 6.7	67.0 ± 7.7
9.0 - 10.0	17.1 ± 2.2	15.2 ± 2.0	14.4 ± 1.8	51.0 ± 6.0	60.2 ± 6.9
10.0 - 11.0	13.2 ± 1.7	12.6 ± 1.7	11.6 ± 1.5	51.8 ± 6.0	52.9 ± 6.0

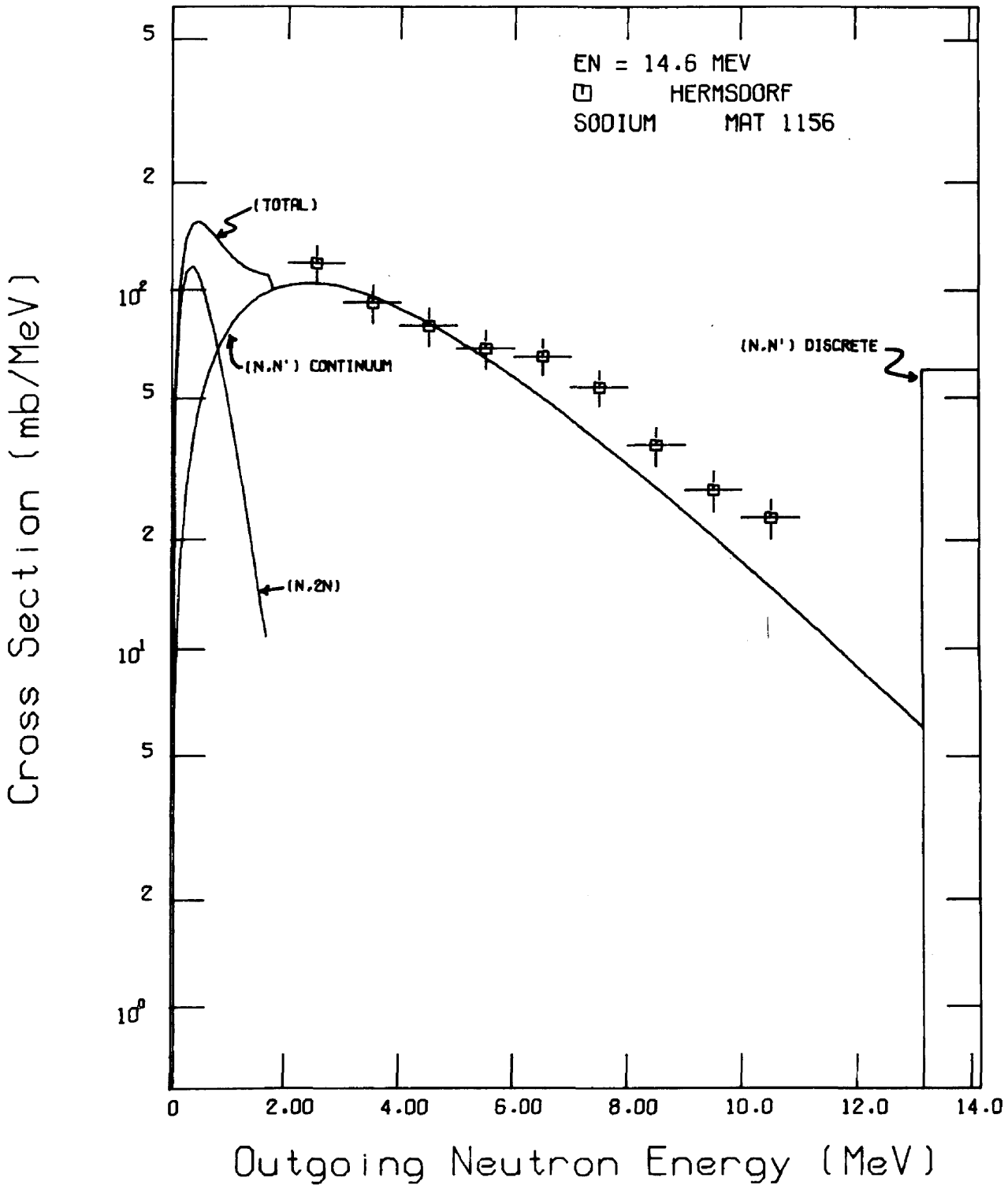

Fig. 1. Partial and Total Neutron Emission Spectra from the ENDF/B-V Files Compared with the Experimental Data of Hermsdorf et al. for the Element Sodium.

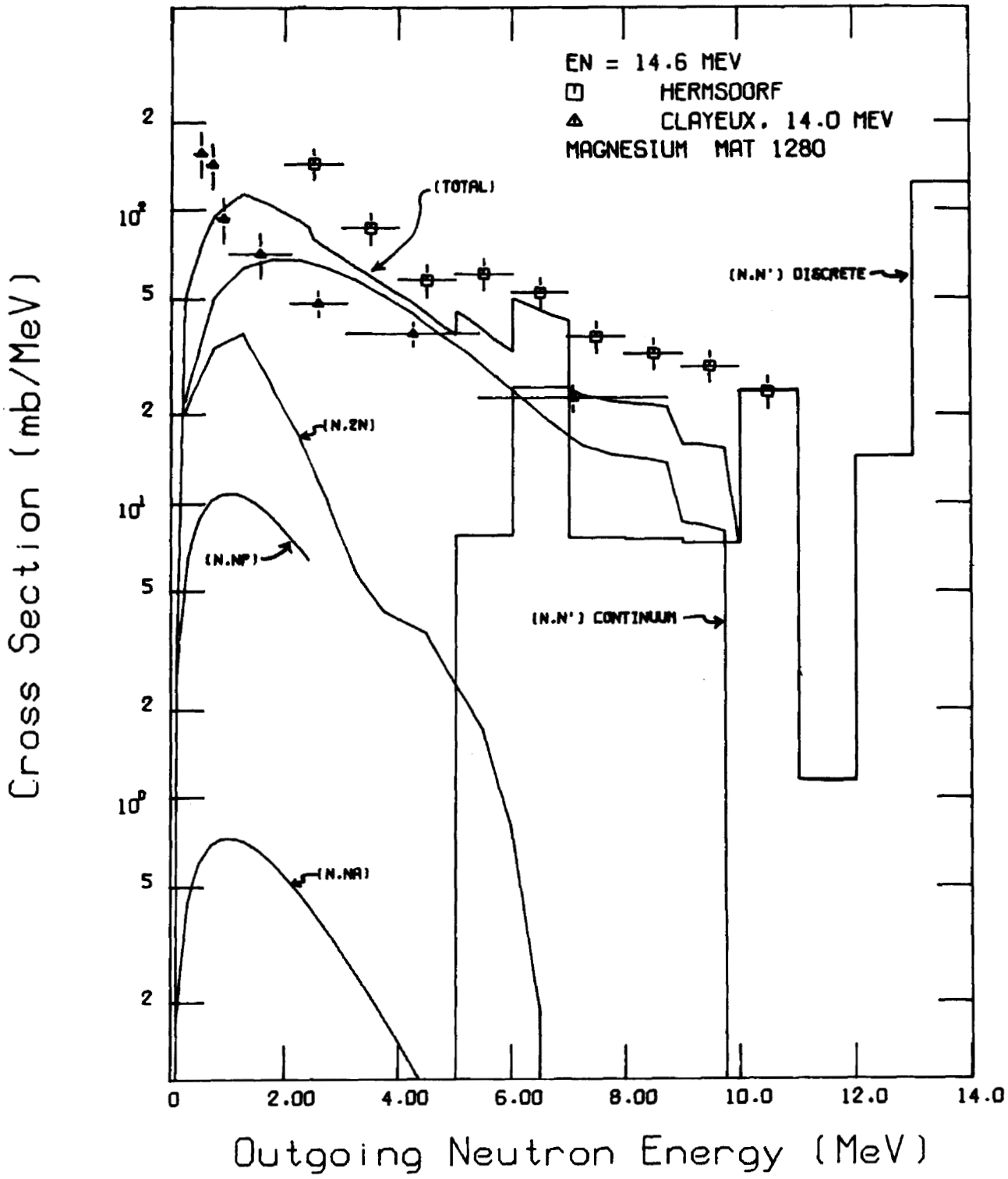

Fig. 2. Partial and Total Neutron Emission Spectra from the ENDF/B-V Files Compared with the Experimental Data of Hermsdorf et al. and Clayeux and Voignier for the Element Magnesium.

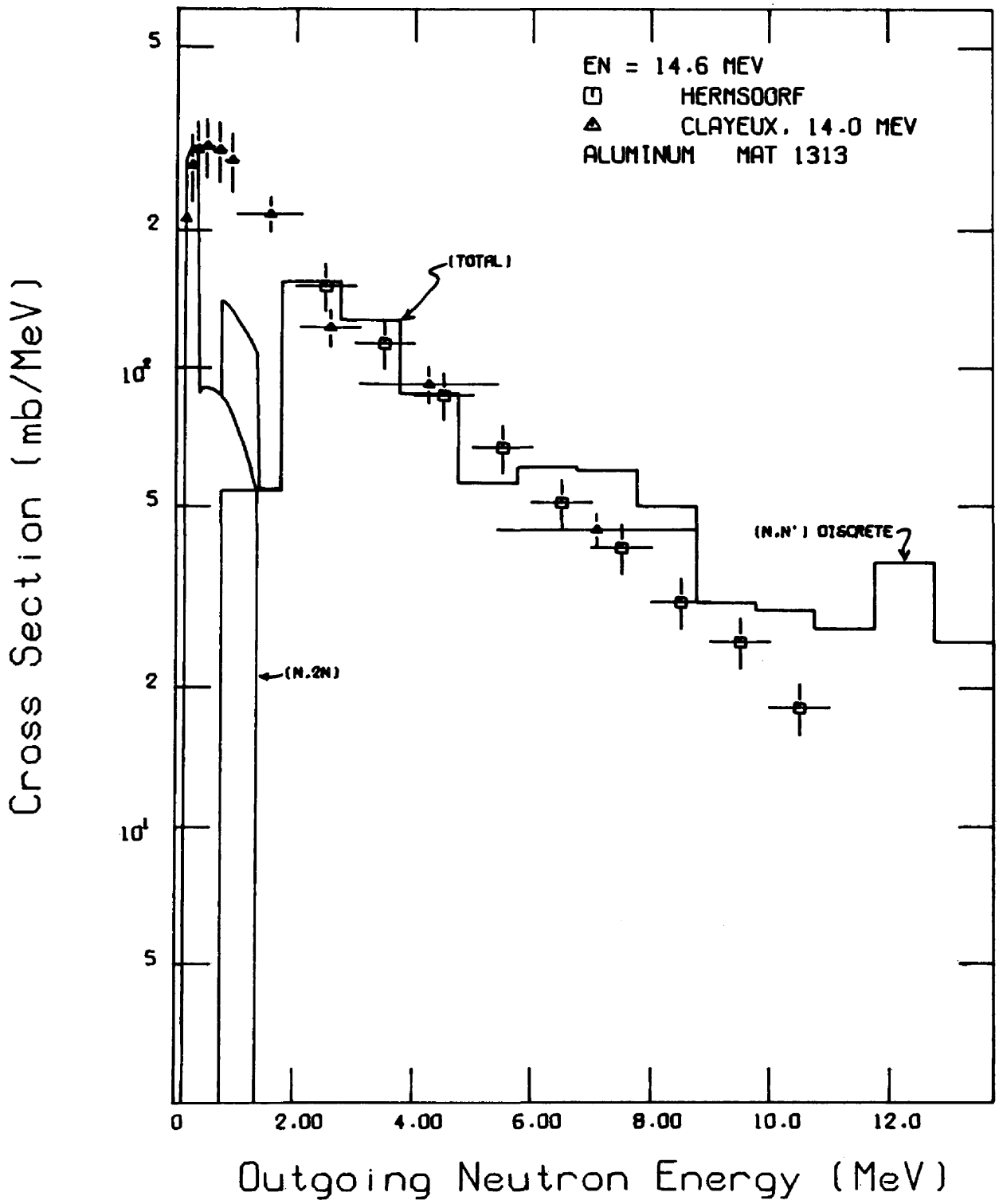

Fig. 3. Partial and Total Neutron Emission Spectra from the ENDF/B-V Files Compared with the Experimental Data of Hermsdorf et al. and Clayeux and Voignier for the Element Aluminum.

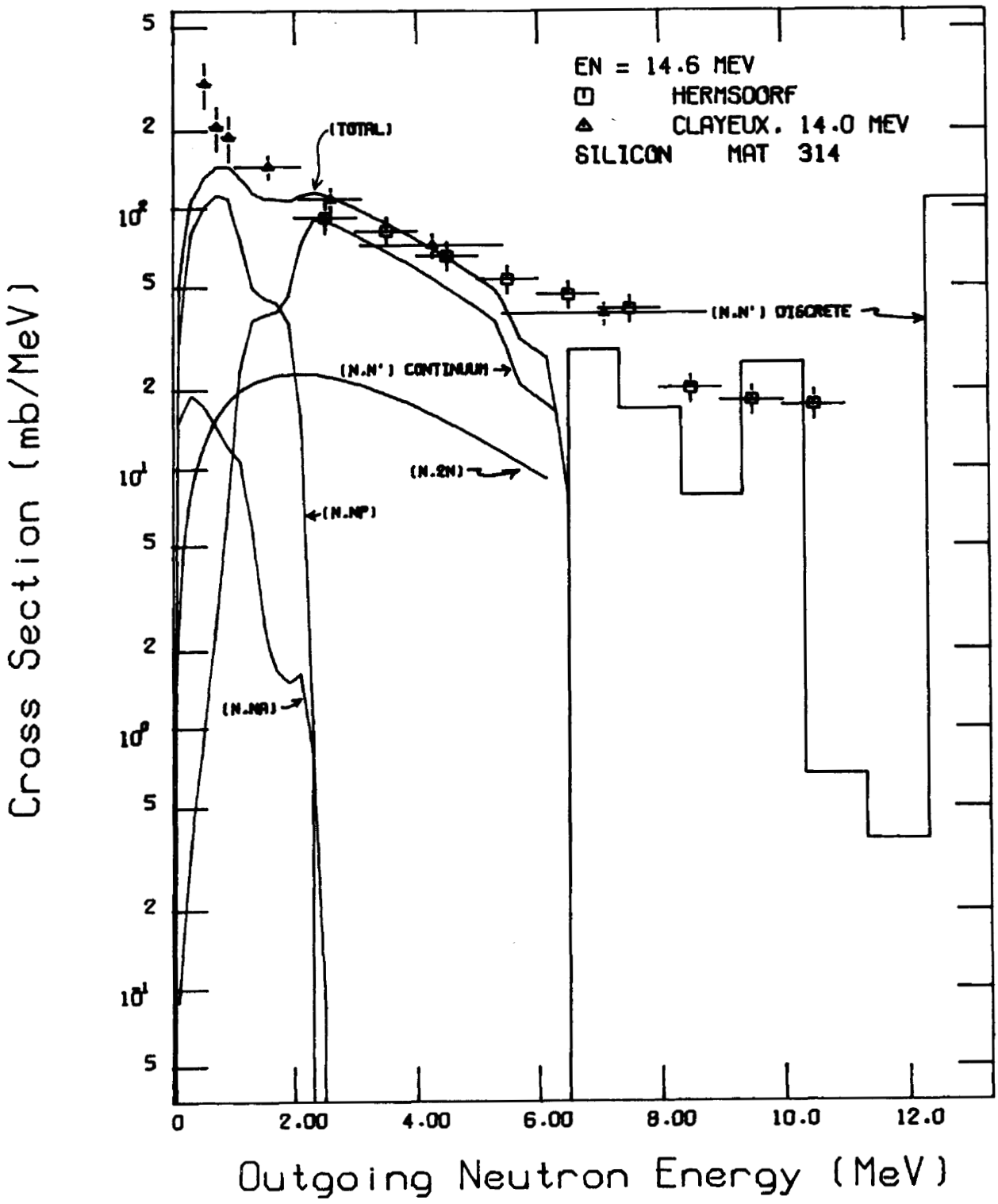

Fig. 4. Partial and Total Neutron Emission Spectra from the ENDF/B-V Files Compared with the Experimental Data of Hermsdorf et al. and Clayeux and Voignier for the Element Silicon.

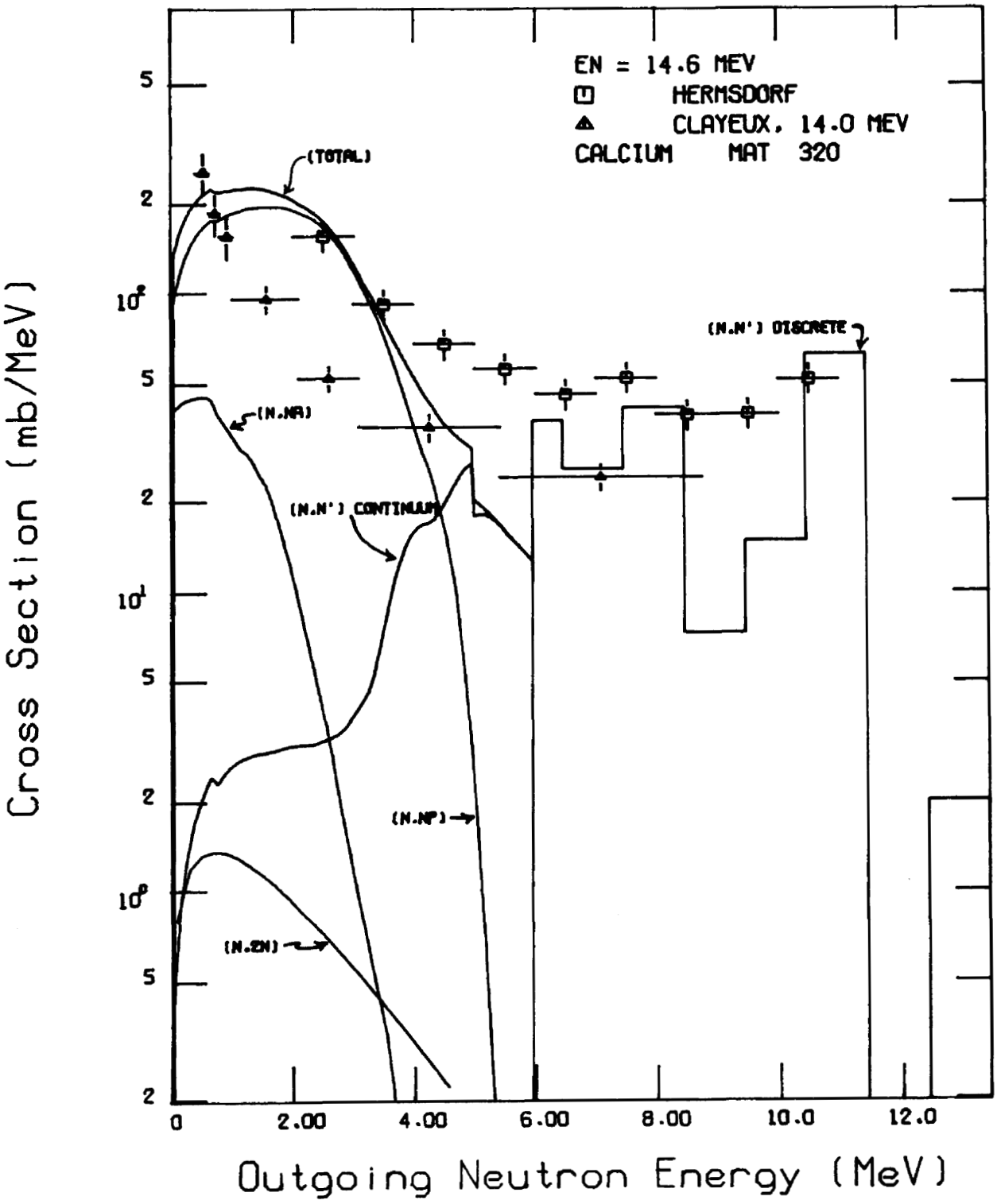

Fig. 5. Partial and Total Neutron Emission Spectra from the ENDF/B-V Files Compared with the Experimental Data of Hermsdorf et al. and Clayeux and Voignier for the Element Calcium.

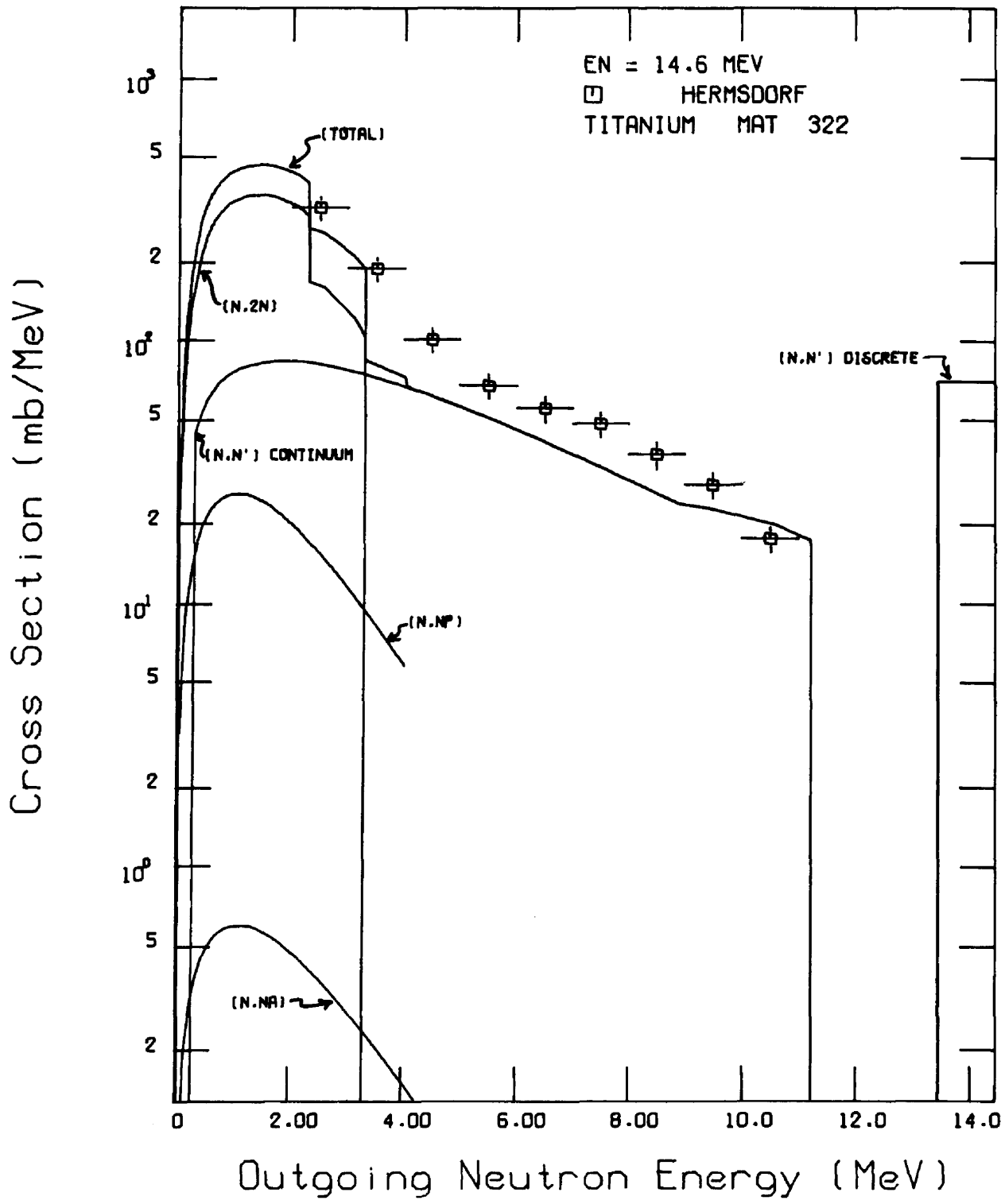

Fig. 6. Partial and Total Neutron Emission Spectra from the ENDF/B-V Files Compared with the Experimental Data of Hermsdorf et al. for the Element Titanium.

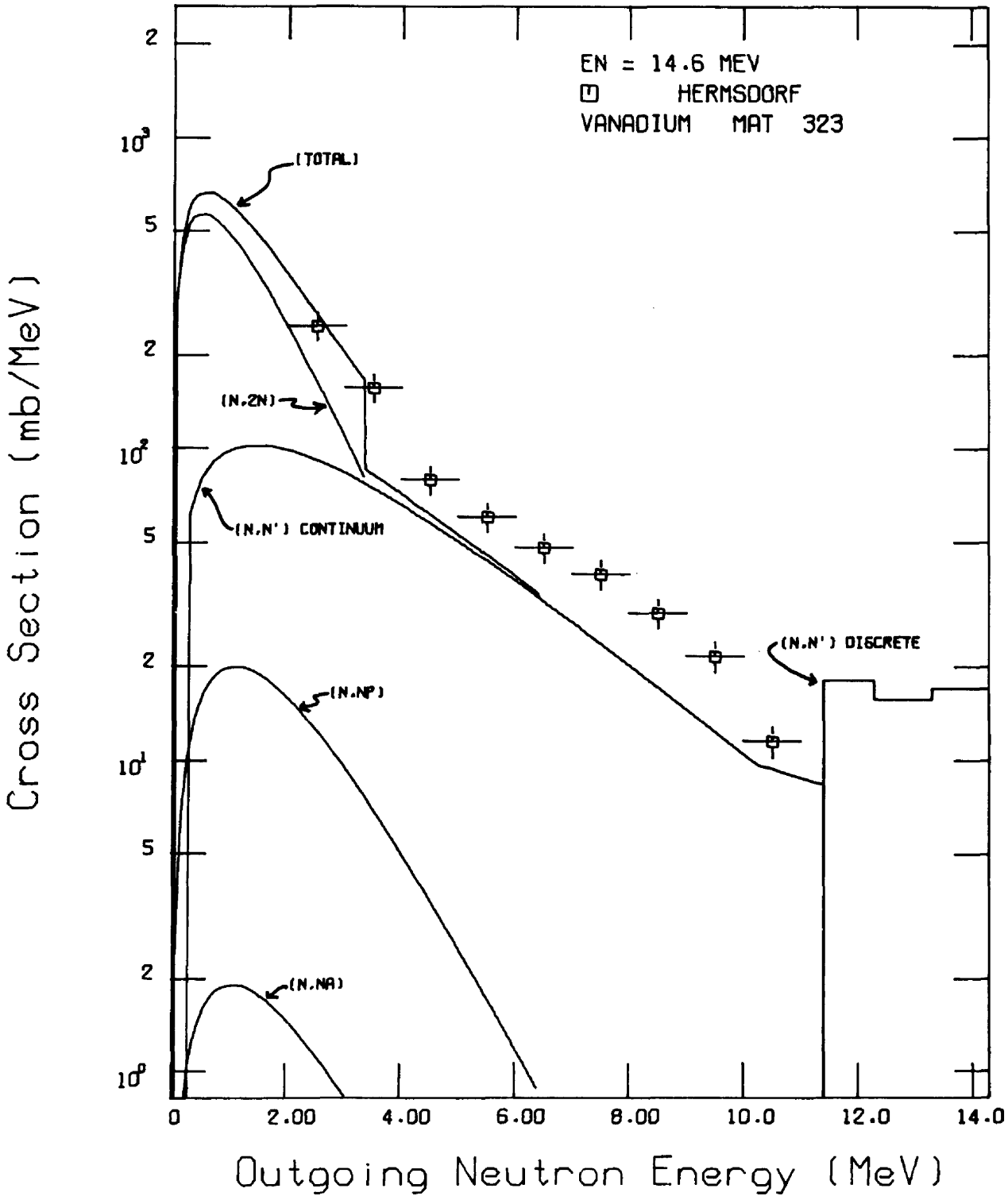

Fig. 7. Partial and Total Neutron Emission Spectra from the ENDF/B-V Files Compared with the Experimental Data of Hermsdorf et al. for the Element Vanadium.

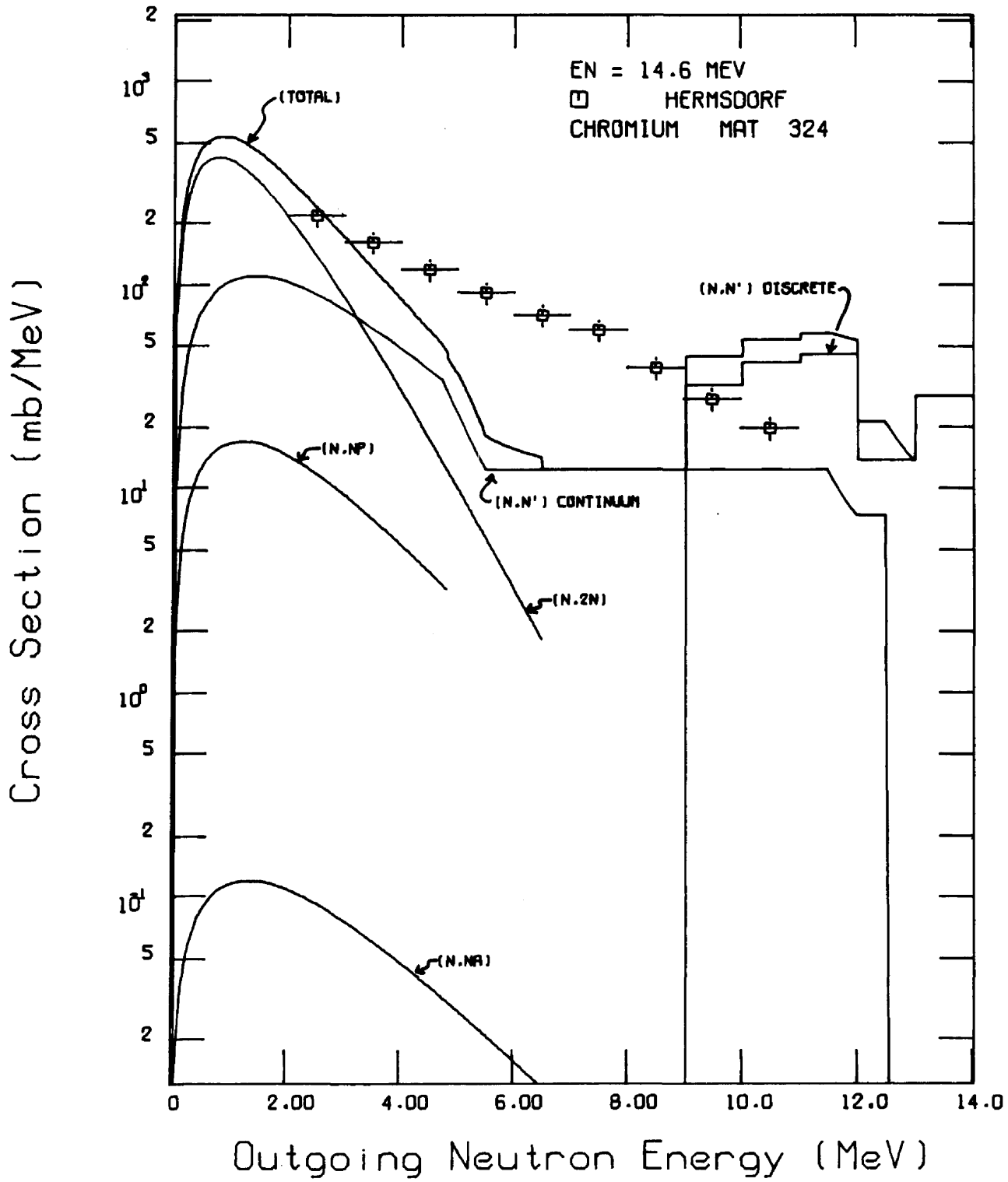

Fig. 8. Partial and Total Neutron Emission Spectra from the ENDF/B-V Files Compared with the Experimental Data of Hermsdorf et al. for the Element Chromium.

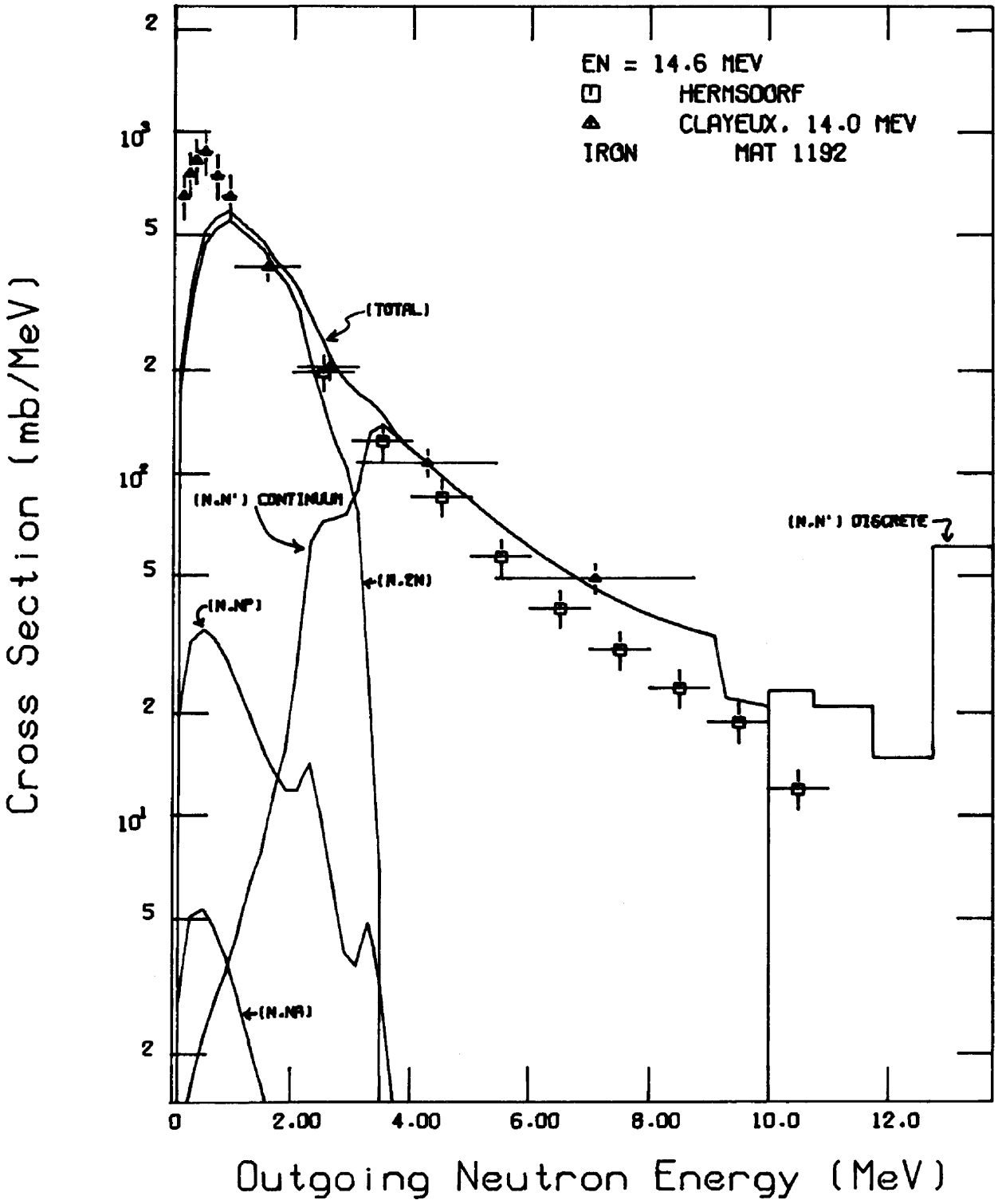

Fig. 9. Partial and Total Neutron Emission Spectra from the ENDF/B-V Files Compared with the Experimental Data of Hermsdorf et al. and Clayeux and Voignier for the Element Iron.

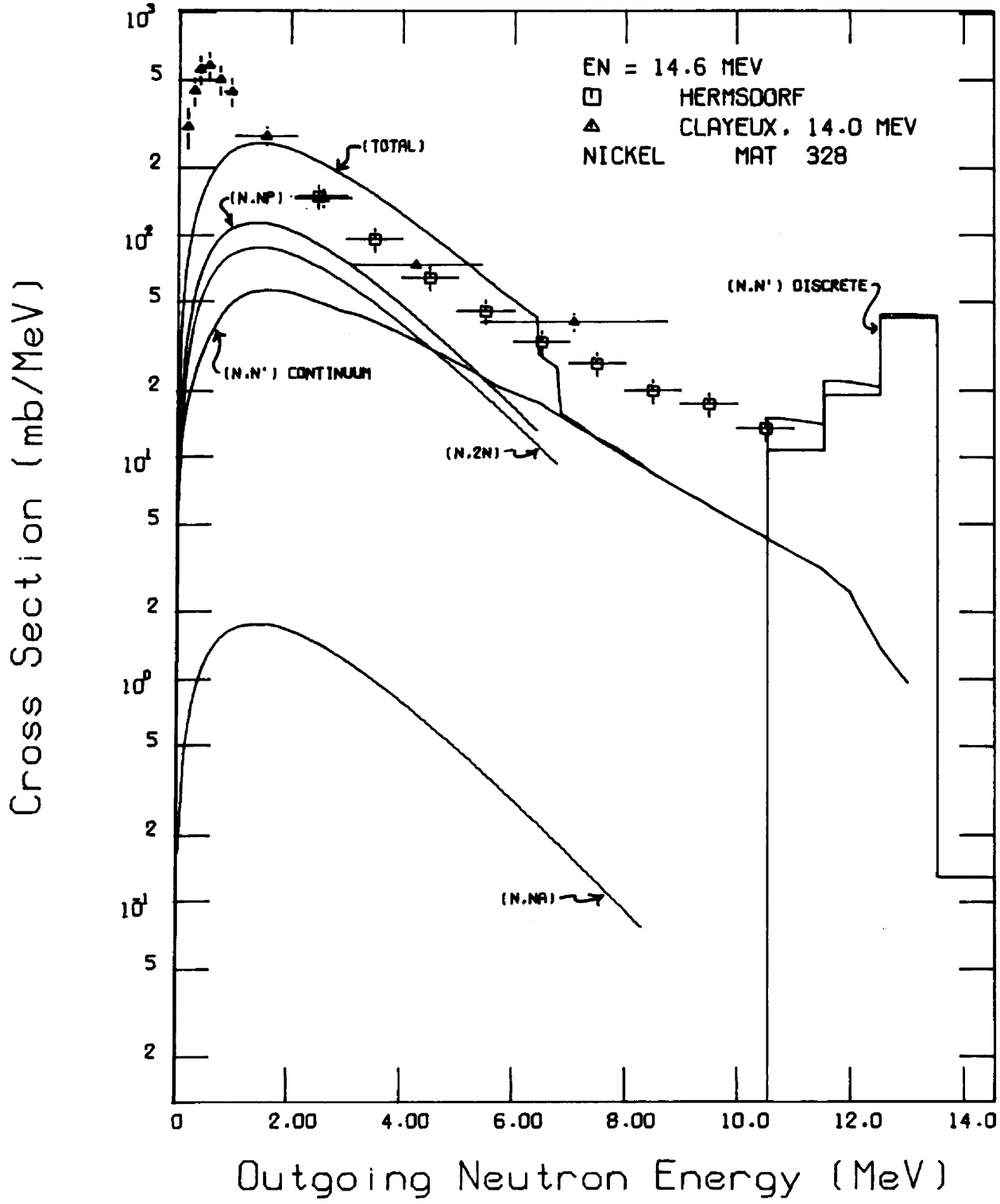

Fig. 10. Partial and Total Neutron Emission Spectra from the ENDF/B-V Files Compared with the Experimental Data of Hermsdorf et al. and Clayeux and Voignier for the Element Nickel.

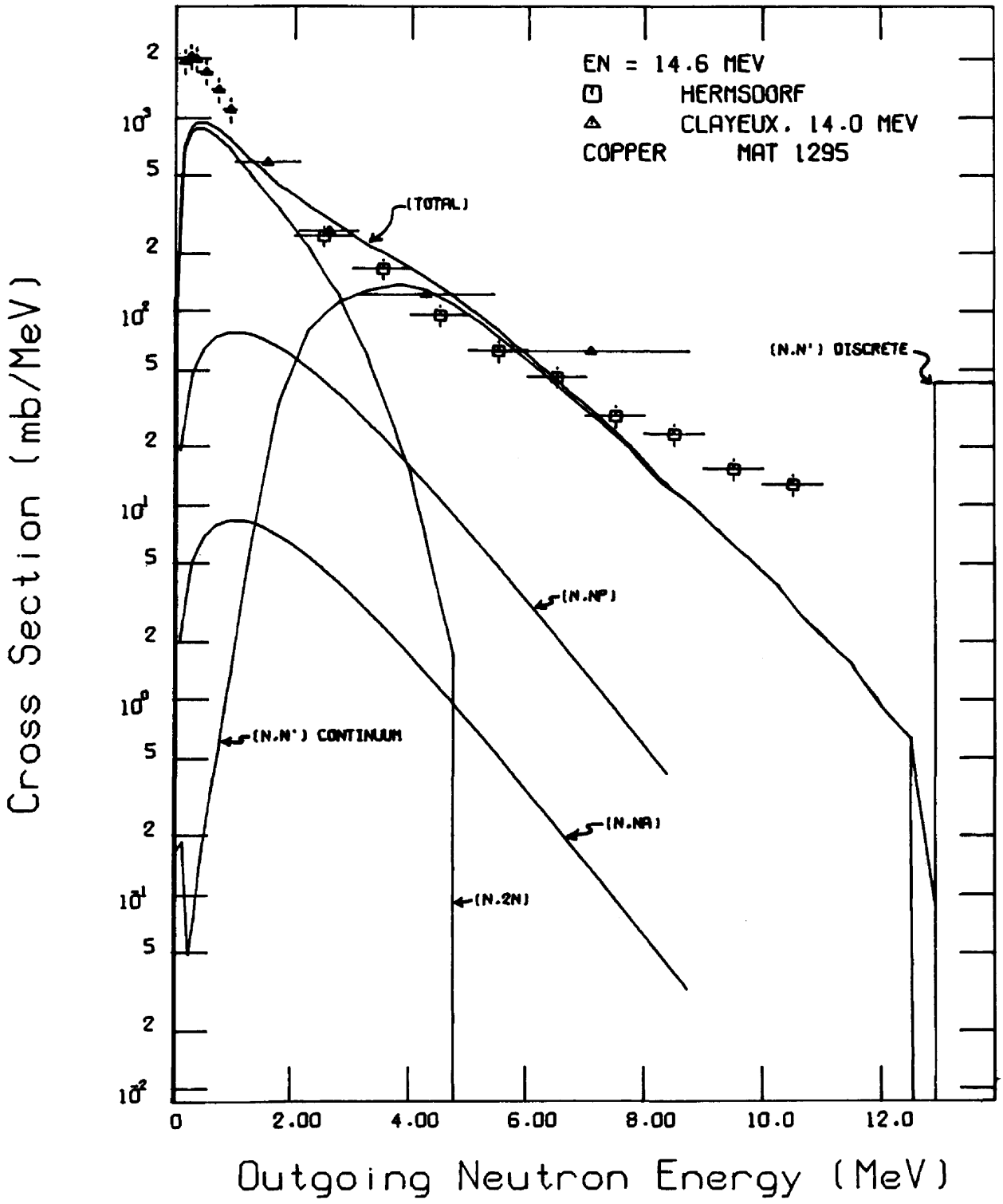

Fig. 11. Partial and Total Neutron Emission Spectra from the ENDF/B-V Files Compared with the Experimental Data of Hermsdorf et al. and Clayeux and Voignier for the Element Copper.

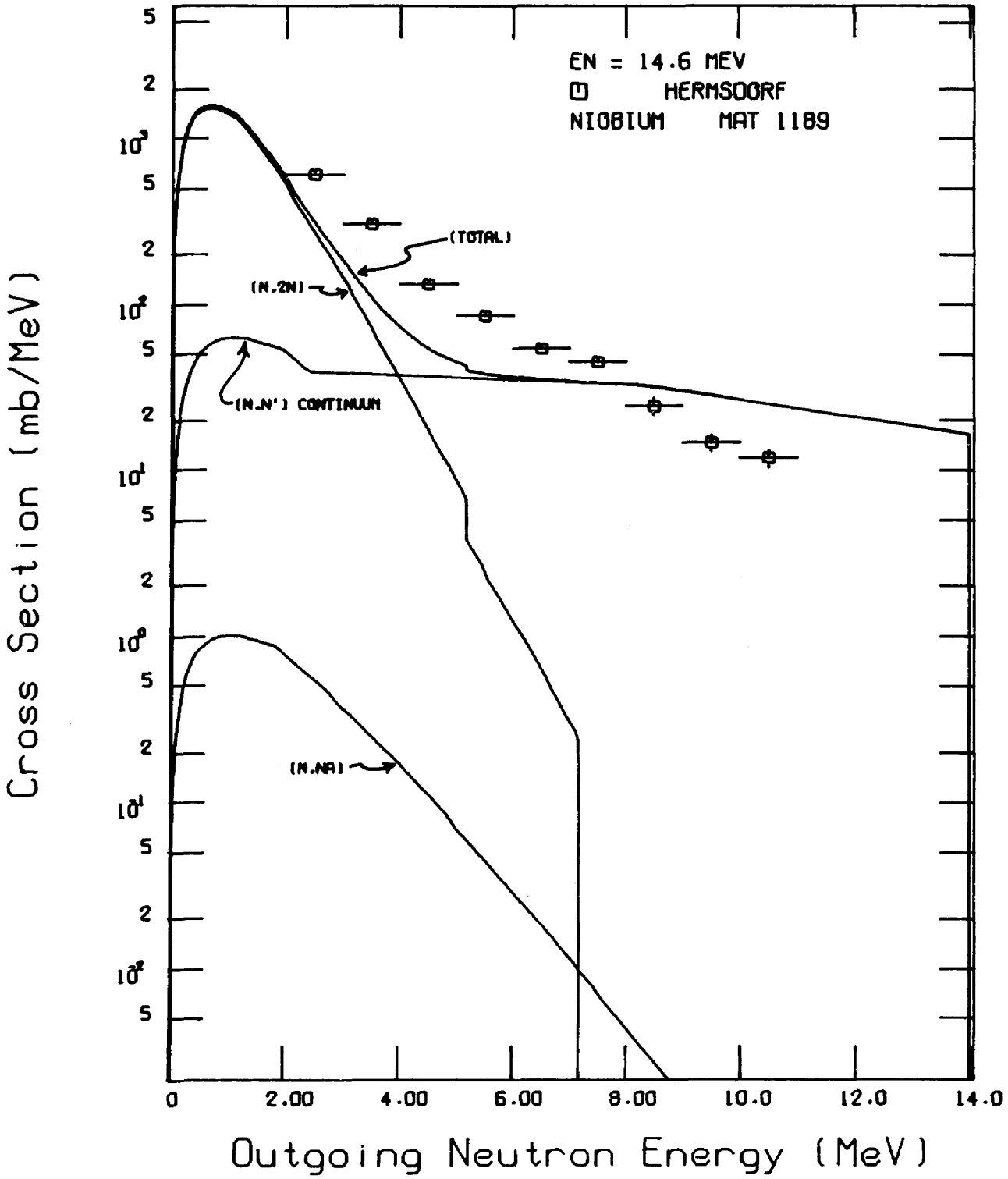

Fig. 12. Partial and Total Neutron Emission Spectra from the ENDF/B-V Files Compared with the Experimental Data of Hermsdorf et al. for the Element Niobium.

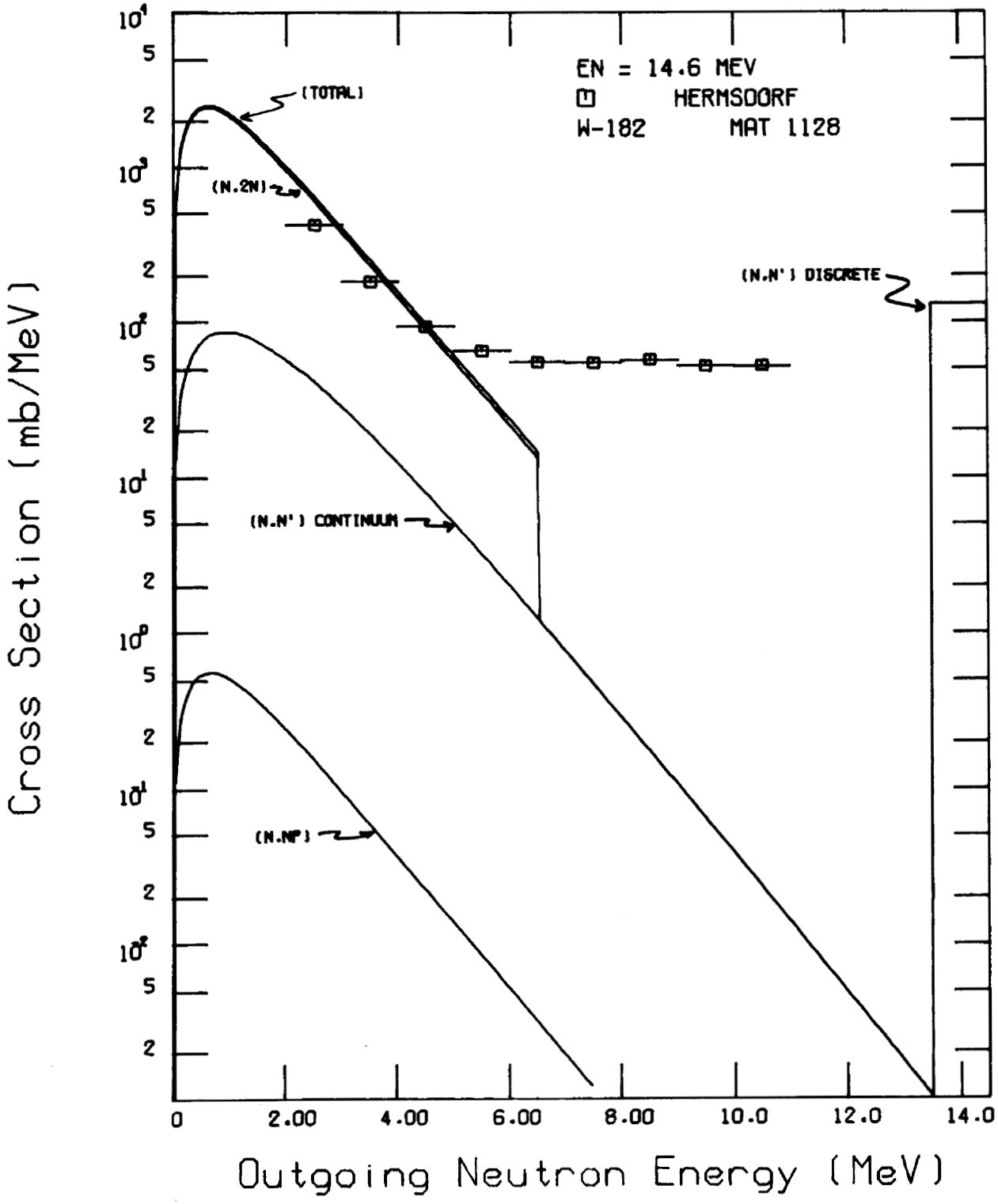

Fig. 13. Partial and Total Neutron Emission Spectra from the ENDF/B-V Files for W-182 Compared with the Experimental Data of Hermsdorf et al. for the Element Tungsten.

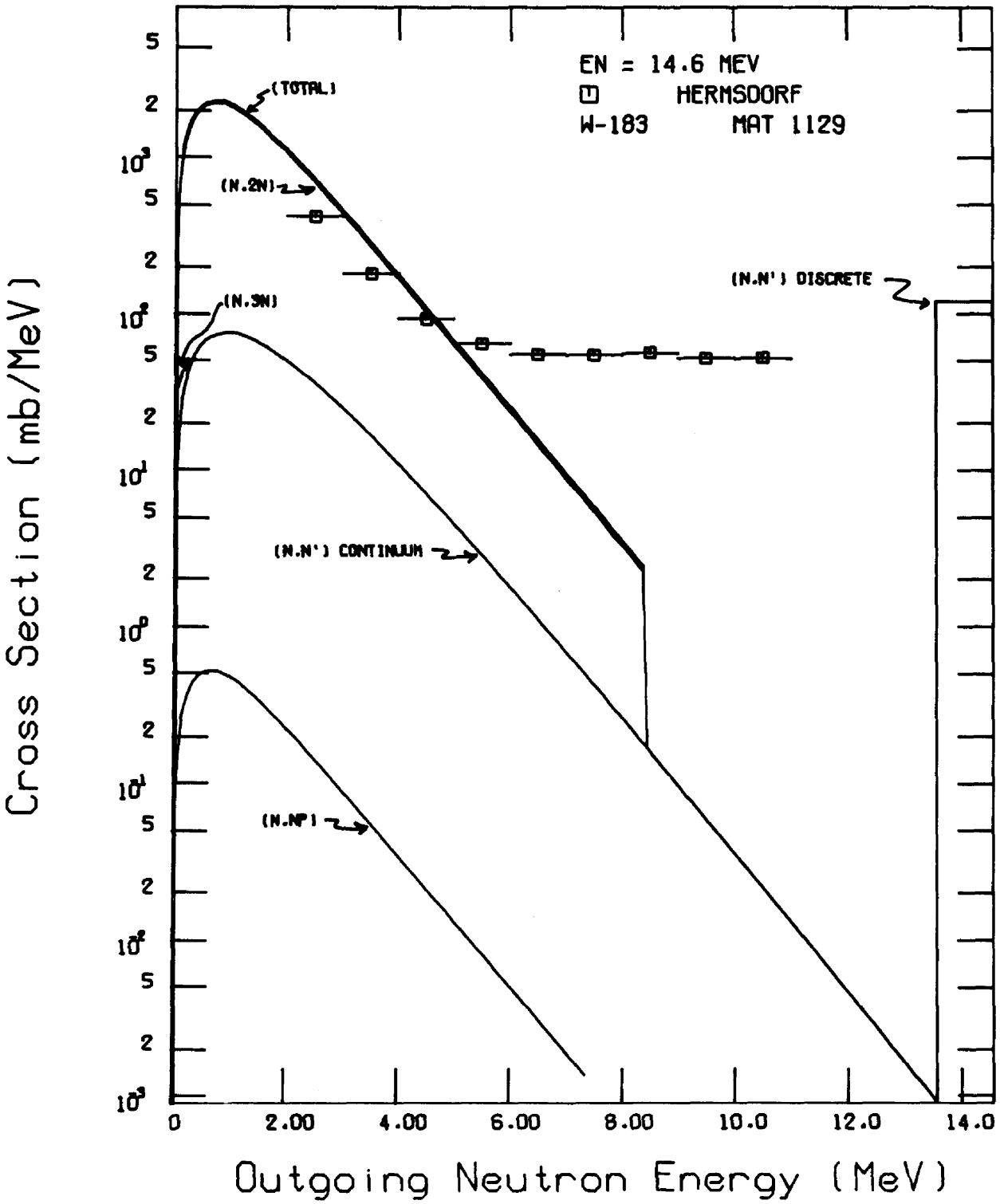

Fig. 14. Partial and Total Neutron Emission Spectra from the ENDF/B-V Files for W-183 Compared with the Experimental Data of Hermsdorf et al. for the Element Tungsten.

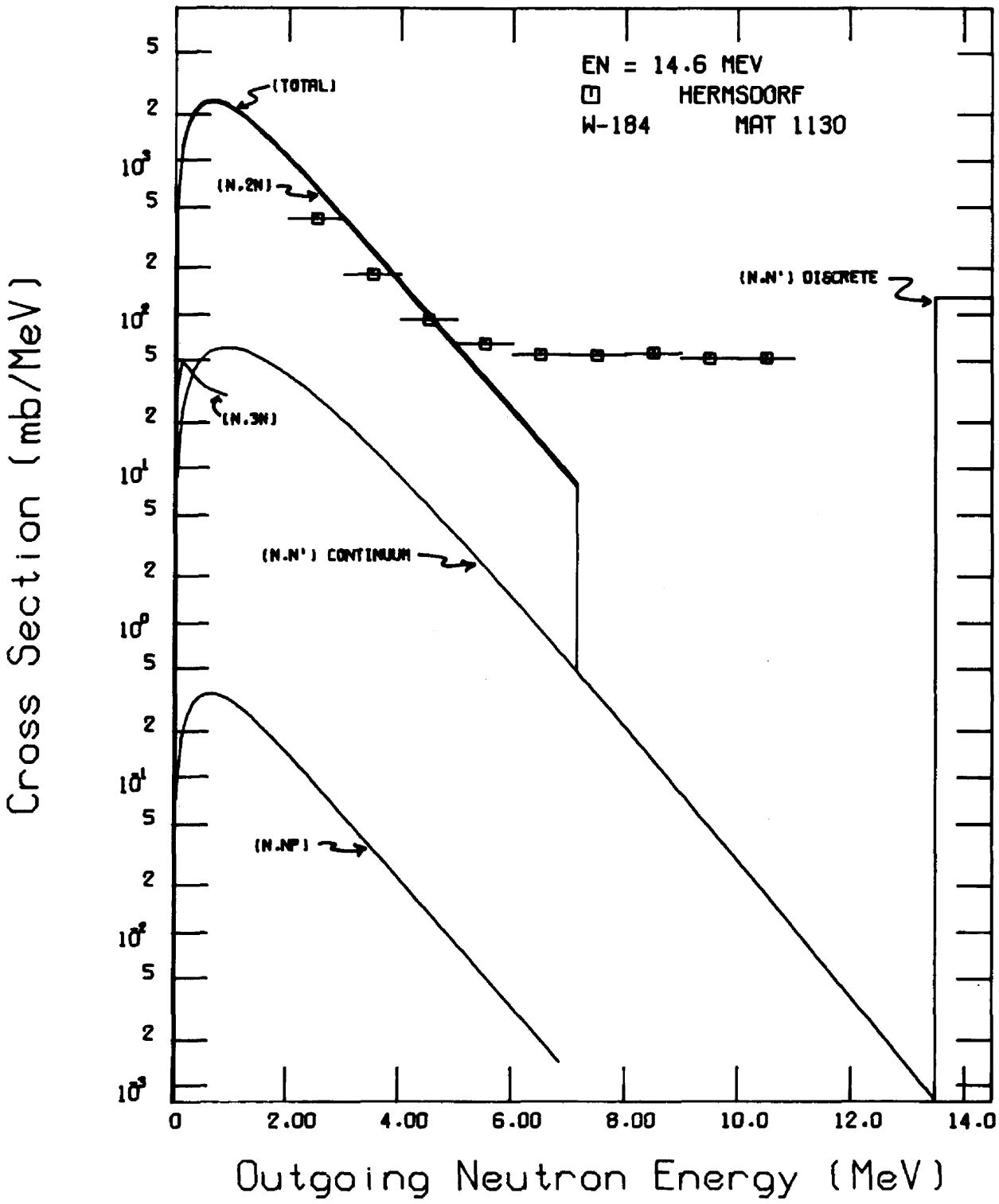

Fig. 15. Partial and Total Neutron Emission Spectra from the ENDF/B-V Files for W-184 Compared with the Experimental Data of Hermsdorf et al. for the Element Tungsten.

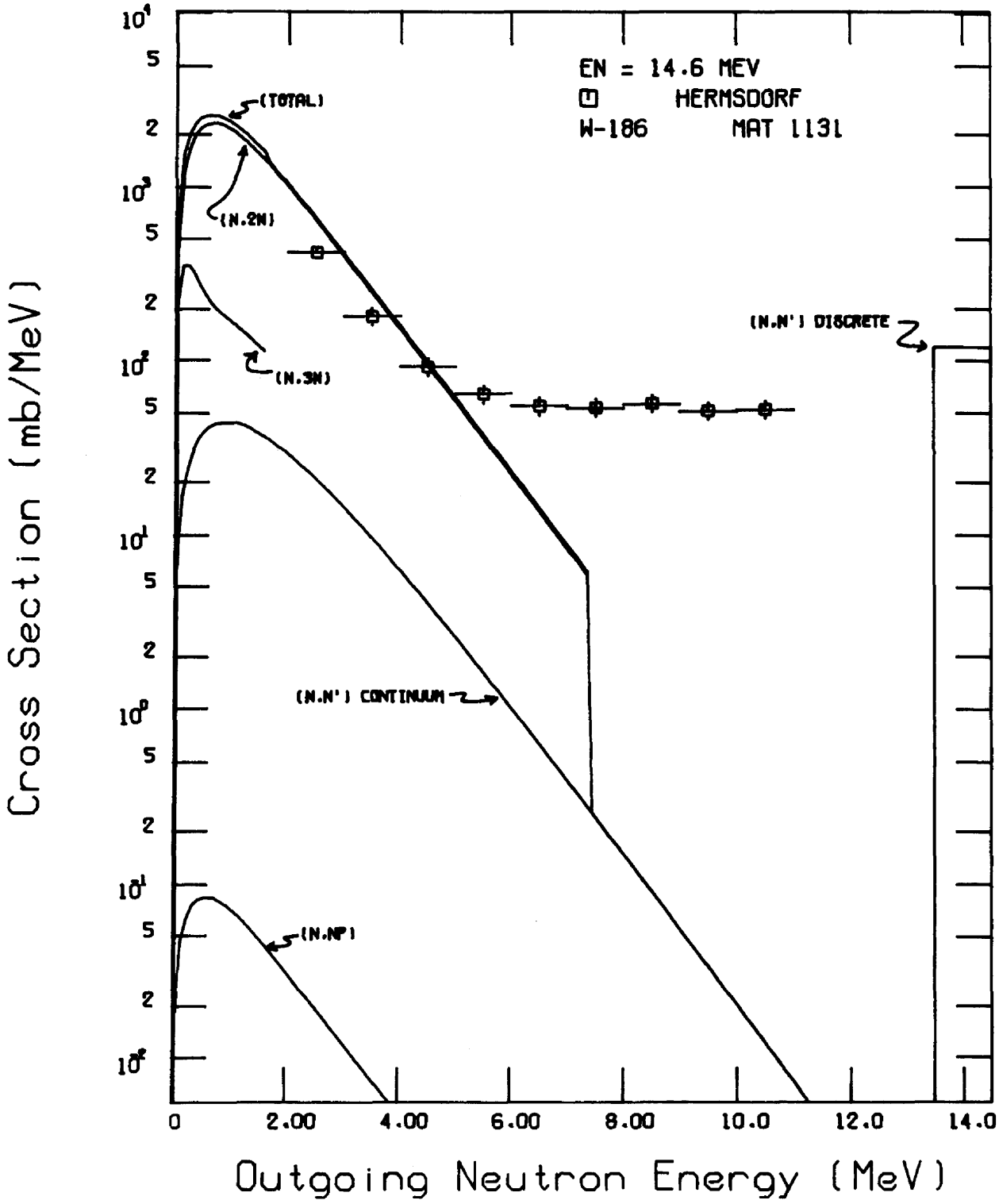

Fig. 16. Partial and Total Neutron Emission Spectra from the ENDF/B-V Files for W-186 Compared with the Experimental Data of Hermsdorf et al. for the Element Tungsten.

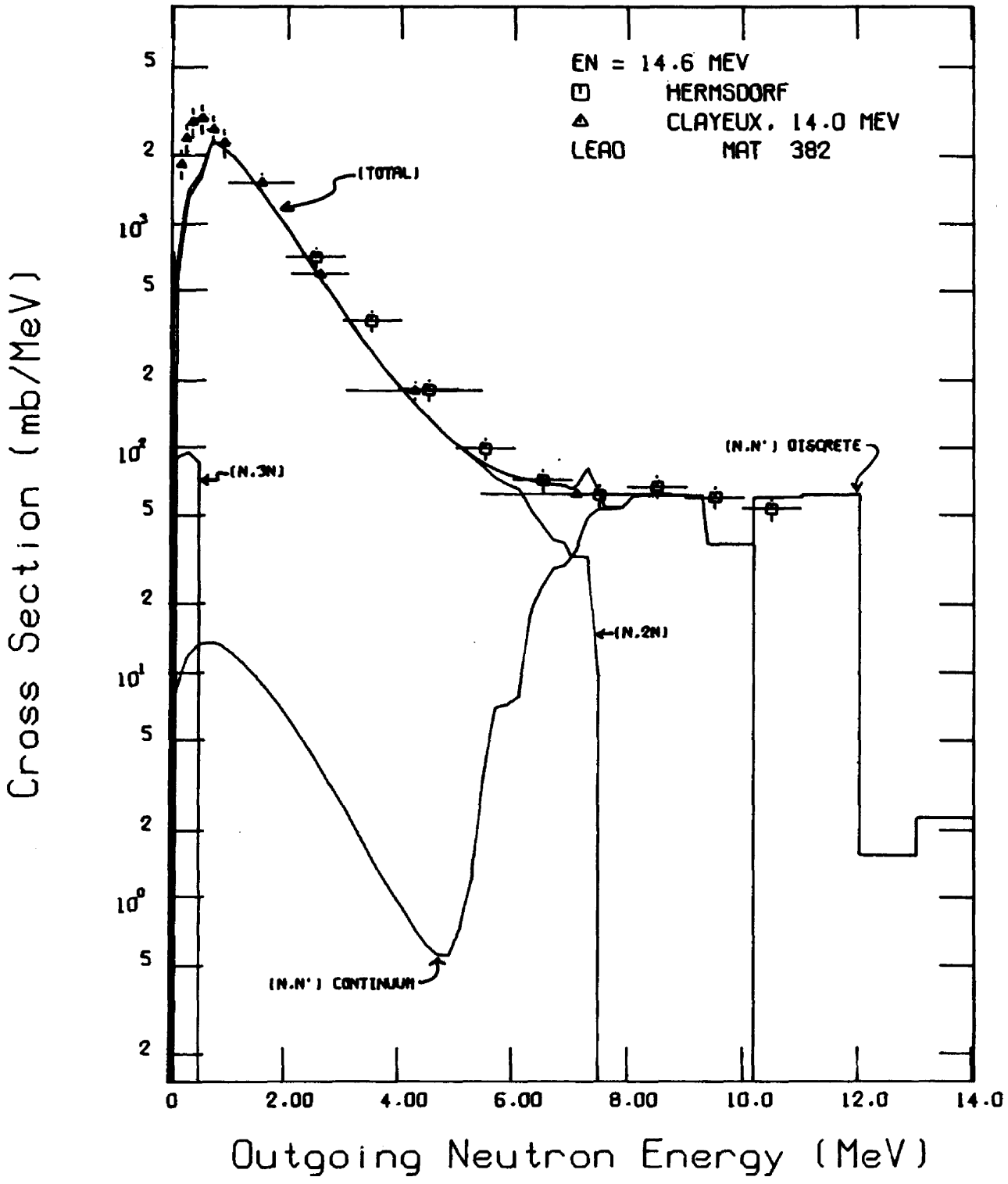

Fig. 17. Partial and Total Neutron Emission Spectra from the ENDF/B-V Files Compared with the Experimental Data of Hermsdorf et al. and Clayeux and Voignier for the Element Lead.

ORNL/TM-6637
ENDF-280

INTERNAL DISTRIBUTION

1. L. S. Abbott
2. R. G. Alsmiller, Jr.
3. C. F. Barnett
4. D. E. Bartine
5. G. T. Chapman
6. J. K. Dickens
7. G. F. Flanagan
8-12. C. Y. Fu
13. H. Goldstein (Consultant)
14-23. D. M. Hetrick
24-28. D. C. Larson
29. F. C. Maienschein
30. O. B. Morgan
31. B. D. Murphy
32. E. M. Oblow
33. D. K. Olsen
34. R. W. Peelle
35. F. G. Perey
36-40. RSIC
41. D. Steiner
42. C. R. Weisbin
43. A. Zucker
44. Paul Greebler (Consultant)
45. W. B. Loewenstein (Consultant)
46. R. E. Uhrig (Consultant)
47. Richard Wilson (Consultant)
48-49. Central Research Library
50. ORNL - Y-12 Technical Library
51. Laboratory Records, ORNL RC
52. ORNL Patent Office
53-54. Laboratory Records

EXTERNAL DISTRIBUTION

55. John D. Anderson, E Division, Lawrence Livermore Laboratory, Livermore, CA 94550
56. H. H. Barschall, Dept. of Physics University of Wisconsin, Madison, WI 53706
57. D. Dudziak, Los Alamos Scientific Laboratory, Los Alamos, NM 87545
58. R. L. Egli, Director, Reactor Division, DOE, ORO
59. S. Gerstl, Los Alamos Scientific Laboratory, Los Alamos, NM 87545
60. R. C. Haight, Lawrence Livermore Laboratory, Livermore, CA 94550
61. C. R. Head, Reactor Systems and Applications Branch, Office of Fusion Energy, DOE, Washington, DC 20545
62. G. L. Morgan, P-3 Division, Los Alamos Scientific Laboratory, Los Alamos, NM 87545
63. D. W. Muir, Los Alamos Scientific Laboratory, Los Alamos, NM 87545
64. R. L. Walter, Dept. of Physics, Duke University, Durham, NC 27706
65. V. J. Orphan, Science Applications, Inc., P.O. Box 2351, La Jolla, CA 92037
66. J. M. Williams, Div. of Controlled Thermonuclear Research, DOE, Washington, DC 20545
67. Office of Assistant Manager, Energy Research and Development, DOE-ORO, Oak Ridge, TN 37830
68-94. Technical Information Center, Oak Ridge
95-183. Mary Rizzi, National Nuclear Data Center, ENDF, Brookhaven National Laboratory, Upton, NY 11973